



# Lightweight deep learning model for automatic landslide prediction and localization

Payal Varangaonkar<sup>1</sup> · S. V. Rode<sup>2</sup>

Received: 26 April 2022 / Revised: 10 August 2022 / Accepted: 27 February 2023

© The Author(s), under exclusive licence to Springer Science+Business Media, LLC, part of Springer Nature 2023

## Abstract

There has been a lot of interest in utilizing remote sensing images to anticipate landslides. We propose a novel framework for automatic landslide detection and landslide region localization from the input remote sensing image. The framework consists of pre-processing, dynamic segmentation, automatic feature extraction, classification, and localization. The pre-processing is the integrated step that performs atmospheric corrections, geometric corrections, and unnecessary region removal with denoising using 2D median filtering. The pre-processed image is then segmented using the dynamic segmentation approach to extract the Region of Interest (ROI). We propose lightweight Convolutional Neural Network (CNN) layers for automatic feature extraction and scaling using the ResNet50 model. The CNN layers are designed systematically for automatic feature extraction to improve accuracy and reduce computational requirements. The Long-Term Short Memory (LSTM), Artificial Neural Network (ANN), and Support Vector Machine (SVM) classifiers are designed to perform the landslide prediction. If landslides are forecast, the post-processing stages are intended to identify potential landslide locations. The experimental results show that the proposed CNN-LSTM model outperformed the existing solutions in terms of accuracy, F1 score, precision, and recall rates. The experimental outcomes reveal that the proposed model improves the overall prediction accuracy by 2% and reduces the computational complexity by 35% compared to state-of-the-art methods.

**Keywords** Computer vision methods · Convolutional neural network · Deep learning · LSTM · Landslide detection · Landslide localization · Segmentation

---

✉ Payal Varangaonkar  
payal.varangaonkar@gmail.com

S. V. Rode  
sandeepode30@gmail.com

<sup>1</sup> Sipna College of Engineering and Technology, Amravati, India

<sup>2</sup> Electronics and Telecommunication Department, Sipna College of Engineering & Technology, Amravati, India

## 1 Introduction

Landslides are among the most harmful natural disasters, destroying houses and infrastructure and killing many innocent people [7]. The International Landslide Center at Durham University in the UK estimates 2620 deadly landslide episodes between 2004 and 2010, killing 32,322 persons [25]. Asia has more landslides than other locations. In Asia, landslides killed around 18,000 people and impacted 5.5 million between 1950 and 2009. China had 695 landslide-related deaths in 2007, according to Durham University's International Landslide Center. India, Indonesia, Bangladesh, Vietnam, and Nepal followed China [29]. In the Himalayas and Vietnam, landslides occur following severe rains, causing human deaths and property and infrastructure damage. Remedial procedures including retaining walls, anchor systems, lowering slope steepness, covering slopes with steel networks, etc. might lessen landslide dangers. Other ways to prevent landslides include reducing the weight on steep slopes, preventing groundwater from rising in slope-forming material, and covering unstable slopes with impermeable membranes [21, 28]. These solutions are only relevant to local or minor unstable slopes. Regional land use planning, decision-making, and early warning systems can decrease landslide frequency and severity. High-risk landslide areas are often discovered through hazard assessment and mapping. Landslide hazard research relies heavily on geo-informatics methods like Remote Sensing (RS) and Geographic Information Systems (GIS) [21, 28, 43, 44].

GIS is a powerful geographical analysis application that also includes graphics image processing and spatial data management capabilities, among other things [44]. The GIS is used to combine and handle all forms of landslide information. When used for landslide monitoring and modeling, remote sensing technologies paired with GIS can perform a variety of functions, including data collection, analysis, evaluation, and visualization [44]. Recently, many GIS-based systems for landslide hazard modeling have been designed [1, 10, 12–14, 17, 23, 26, 31, 33, 34, 39]. Many of which incorporate machine learning approaches such as Fuzzy Logic [1, 39], Neuro-Fuzzy [23, 33, 34], ANN [12–14], SVM [26, 31], and Decision-Tree Models [10, 17]. Many studies [19] made use of RS images for landslide prediction, detection, and localization, employing a variety of image processing and machine learning algorithms to achieve success. It was possible to spot changes in landslide images taken before and after the disaster by employing several techniques such as thresholding, binary temporal methods, texture analysis, etc. [19]. Although all of these methods [1, 10, 12–14, 17, 23, 26, 31, 33, 34, 39] were capable of scaling up to large numbers of image graphs, they suffered from significant limitations. As such methods used to evaluate conventional images could not be directly applied to RS images, it significantly results in poor accuracy and efficiency. Similarly, we have studied some other domain prediction methods [3, 4] during this study. The RS-based image processing techniques [6, 16, 20, 45] have recently been presented using various computer vision methods.

Predicting landslides with RS images has gained popularity since it uses real-time visual data. Lack of data and expertise about landslide locations, especially in western and northern India, poor methodologies for interpreting landslide images, erroneous landslide evaluations, and challenging localization of landslide changes are hurdles [32]. Landslide prediction or localization using artificial characteristics or spatial information fails because it's hard to construct spatial regularities exclusively associated with landslides. The current study offers a thresholding approach for autonomous landslide identification [11]. Improved landslide prediction and localization are needed. Using machine learning and deep learning, early

landslide prediction is possible. The machine learning methods heavily relied on handcrafted features, whereas the deep learning models automatically extract the features using the pre-trained models [22]. Therefore, deep learning delivered a more efficient and user-friendly approach compared to machine learning techniques [8].

The automated prediction of landslides ensures that proper attention is paid to avoiding financial and human losses. Deep learning takes a longer duration to complete dataset training and detection since it is a completely automated feature learning and extraction approach. As a result, such solutions are not reliable and scalable to process large datasets. The reliability of using deep learning models is affected by higher prediction time. The system becomes unreliable as the decision-making system has to wait for a longer time. The long training duration using deep learning also affects the scalability as larger datasets require high computational efforts. Because of its improved accuracy and feature representation, deep learning techniques such as convolutional neural networks (CNN) have gained popularity for a variety of applications [8, 11, 22, 32, 36]. However, computational complexity is a significant research issue when employing CNN. Because each RS image has a high-dimensional feature space, CNN has greater computational complexity.

Novel lightweight 2D CNN layers are proposed in this paper for the automatic feature extraction from the ROI RS image. The high-dimensional feature space is then normalized using the appropriate scaling technique to enhance the prediction accuracy. The proposed CNN layers are designed in such a way that it reduces the overall computation efforts while ensuring higher accuracy. Before CNN, we performed the pre-processing of RS images using the Normal Digital Vegetation Index (NDVI). The corrected RS image is then segmented using a dynamic thresholding mechanism. The normalized features of CNN are fed to the different classifiers SVM, KNN, and LSTM. The post-processing phase of the proposed model is designed to localize the landslide predicted regions in the input RS image. The remainder of the paper consists of the below sections. Section 2 described the related works on landslide prediction. Section 3 presented the detailed methodology of this paper. Section 4 presented the simulation results and analysis. Section 5 presented the conclusion and suggestions.

## 2 Related works

Due to global warming, seasonal and non-seasonal heavy rainfalls become challenges to the universe. The challenges become severe in the rainfall regions. Thus, it becomes essential to have an automated mechanism that periodically analyzes such landslide hazards and intimate the warnings to save the losses. The GIS and RS satellite information are used to monitor the possible prediction of landslides. This section presents the recent studies [2, 5, 9, 15, 18, 24, 27, 30, 35, 37, 38, 40–42, 46] for landslide prediction using machine learning and deep learning techniques.

### 2.1 Machine learning methods

Landslides were identified using multi-scale image segmentation and machine learning algorithms in recent research [37]. They suggested a unified system for landslide detection that combined item-based image analysis (OBIA) with machine learning (ML)

methodologies such as multilayer perception neural community (MLP-NN), random forest (RF), and logistic regression (LR). Before employing device learning algorithms, the multi-scale segmentation methodology was established. In [24], the authors have offered another innovative OBIA-based solution for landslide detection using LiDAR-derived data. However, the author feels that using the OBIA approach to identify agricultural landslides remains difficult. Because of restricted terrain vision in forest areas and a lack of high-resolution DEM data, while analyzing landslides, the categorization is incorrect. Their technique of detection failed to correctly and completely identify the landslide. Using publicly available geodatabases, machine learning and deep learning techniques were used to detect landslides [42]. Geological, topography, and rainfall data were collected for the landslide analysis. They used classifiers like SVM, random forest, logistic regression, and CNN directly. A lack of adequate computer vision techniques limited the accuracy performance. To reduce the computational dimension and balance the generalization of the model and learning power, a landslide prediction approach based on improved principal component analysis (PCA) and the least-squares supports vector regression (LSSVR) model had described in [15]. The lack of RS image pre-processing and ROI extractions, however, restricts the effectiveness of this method. Introduced two road features in [46], road profile and road aspect, to increase the accuracy of landslide susceptibility mapping by accounting for the influence of landslide movement direction on road. To detect landslides on a given dataset, they used a random forest classifier. To evaluate the performance of U-Net and machine learning methods for automated landslide identification in the Himalayas, two datasets were created [18]. A small dataset of 239 samples was obtained from six training zones and one testing zone to investigate the performance of the fully convolutional U-Net model, random forest, SVM, and KNN classifiers. The scalability of the recommended classifiers had not supported by the small sample set. Due to a lack of appropriate computer vision algorithms, the accuracy performance had restricted. Another recent study [30] used five classifiers to assess landslide vulnerability and regional difference throughout the whole Qinghai-Tibetan Plateau (QTP) region: SVM, random forest, logistic regression, naive Bayes, and deep neural network (DNN). It has the same limitations as [15, 18, 24, 30, 37, 42, 46].

## 2.2 Deep learning methods

In [41], the NDVI and Near-Infrared Spectroscopy (NIRS) methods were applied to the RS images for the pre-processing before applying the CNN for the prediction. The band values indicating the changing features of the landslide were found by integrating the red, green, blue, and near-infrared bands of the pre-landslide remote sensing images with the 4 bands of the post-landslide imagegraphs and NDVI images to create images with 9 bands. CNN had designed to detect landslides. The authors of [40] concentrated on merging the most recent image recognition algorithms with the finest publicly accessible satellite images to develop a system for landslide risk reduction utilizing the 3D CNN model. In [5], the landslide localization mechanism had designed using the CNN and image transform techniques. A CNN had utilized to categorize satellite images that contained landslides. To effectively detect landslides under diverse illumination situations, the transformation technique Hue – Bi-dimensional empirical mode decomposition (H-BEMD) was suggested to calculate the landslide region and magnitude from categorized landslide images. In [2], the CNN-DNN

model had designed for mapping landslide susceptibility. They analyzed CNN-DNN in the Iranian region of Isfahan, which had never been tested on such a large scale before. The proposed model had trained and validated utilizing datasets comprising pertinent data on past landslides, RS images and field reports, and a variety of geology, geomorphological, human activity, and environmental variables as covariates. The distant domain transfer learning (DDTL) had proposed in [27] for the detection and classification of landslides. The scene categorization had originally used in the landslide detection job for satellite image classification. The attention mechanism to DDTL (AM-DDTL) had used to extract information from satellite images more successfully. In [35], a new landslide detection method based on an unsupervised deep learning model had developed. To cope with the challenge of minimal labeled data for training, the authors created an unsupervised learning model using a convolutional auto-encoder (CAE). Without requiring training data, the CAE had used to learn and extract abstract and high-level features. In [38], CNN and Recurrent Neural Network (RNN) were applied for the landslide susceptibility mapping using the dataset of Iran landslide regions. Both CNN and RNN algorithms were designed to produce the susceptibility maps of the landslide using the available training data. To detect landslides, recently the deep learning technique was integrated [9] with rule and object-based image analysis (OBIA). The ResU-Net model was designed and evaluated using the Sentinel-2 dataset.

### 2.3 Problems identification

In the above section, we have reviewed the recent machine learning and deep learning-based techniques for landslide prediction from the input RS images. The main problems of recent studies are summarized below.

- The machine learning-based methods [15, 18, 24, 30, 37, 42, 46] delivered the landslide prediction with poor accuracy and reliability performances, but it takes minimum computational requirements. The deep learning-based studies [2, 5, 9, 27, 35, 38, 40, 41] delivered the complete automated approach to landslide prediction with improved accuracy but suffered from high computational requirements.
- The availability of real-time data is a serious difficulty, particularly in India's landslide zones. There is a lack of prominent and scalable Indian landslide RS images datasets that includes landslide and non-landslide data of the same area in different time series.
- The majority of previous landslide prediction techniques were applied straight to sensor images, with no atmospheric modifications, geometric corrections, or superfluous regions removed. Estimates of changing landslide characteristics were not retrieved successfully, affecting total accuracy.
- The landslide prediction with the accurate localization of the landslide regions in the input RS images is another limitation of the existing methods.

### 2.4 Contributions

We proposed a novel and automatic landslide prediction and localization framework using the lightweight deep learning model and computer vision techniques. The novelty of the proposed model is described in the below contributions.

- We collected the scalable real-time pre-landslide and post-landslide RS images of western India landslide regions (Maharashtra and Goa) directly from the Linear Imaging Self Scanning (LISS-3) satellite in the Bhuvan web portal “<https://bhuvan.nrsc.gov.in/home/index.php>”.
- We constructed the pre-processing and dynamic segmentation stages to perform geometric and atmospheric correction, noisy content removal, and extraction ROI utilizing multiple bands to predict the changing landslide features from the input RS image.
- We proposed the lightweight integrated deep learning model for the automatic features extraction and prediction using CNN (for features extraction) and LSTM (for classification). The proposed CNN-LSTM model addresses the challenges of higher computational time and error rates.
- After the landslide has been predicted, a post-processing phase is suggested to localize the landslide areas in the input ROI image utilizing morphological operations and the results of dynamic segmentation.
- The performance of the proposed framework CNN-LSTM is measured by dividing the collected dataset into 70% training and 30% testing and evaluated with other classifiers ANN and SVM

### 3 Proposed methodology

In this section, we discuss the design and methods of the proposed autonomous landslide prediction and localization framework. Figure 1 shows the overall functionality of the proposed framework that consists of core blocks such as preprocessing, ROI extraction, automatic feature extraction, prediction, and localization. Before these stages, we gathered real-time RS images of the Western India research region into two categories: pre-landslide (normal) and post-landslide (affected). Each RS image consists of four bands such as R, G, near-infrared (NIR), and shortwave infrared (SWIR). The collected real-time dataset has been divided into training and testing. As shown in Fig. 1, the acquired RS image is first preprocessed to produce the NDVI output image. To extract the ROI-specific features, we segmented the NDVI image using dynamic thresholding and morphological operations. The automatic features of the ROI image are extracted using the pre-trained ResNet50 model of CNN. We designed lightweight CNN layers such as the 2D convolutional (Conv.) layer, ReLU layer, max-pooling layer, and scaling layer (additionally designed) to reduce the overall training and testing time. The extracted automatic features are directly fed to another deep learning algorithm, LSTM, sequentially for the prediction of the landslide possibilities from the input RS images. If the predicted outcome is the possibility of a landslide, then we perform the postprocessing operations to localize the affected landslide regions in that area.

#### 3.1 Study area and dataset

The study area is in western India's Konkan region. The Konkan area runs for around 100 km along with Maharashtra's, Goa's, and Karnataka's western coasts. The Western Ghats Mountain range borders it on the east, the Arabian Sea on the west, the Daman Ganga River on the north, and the Aghanashini River on the south. The RS samples came straight from the LISS-

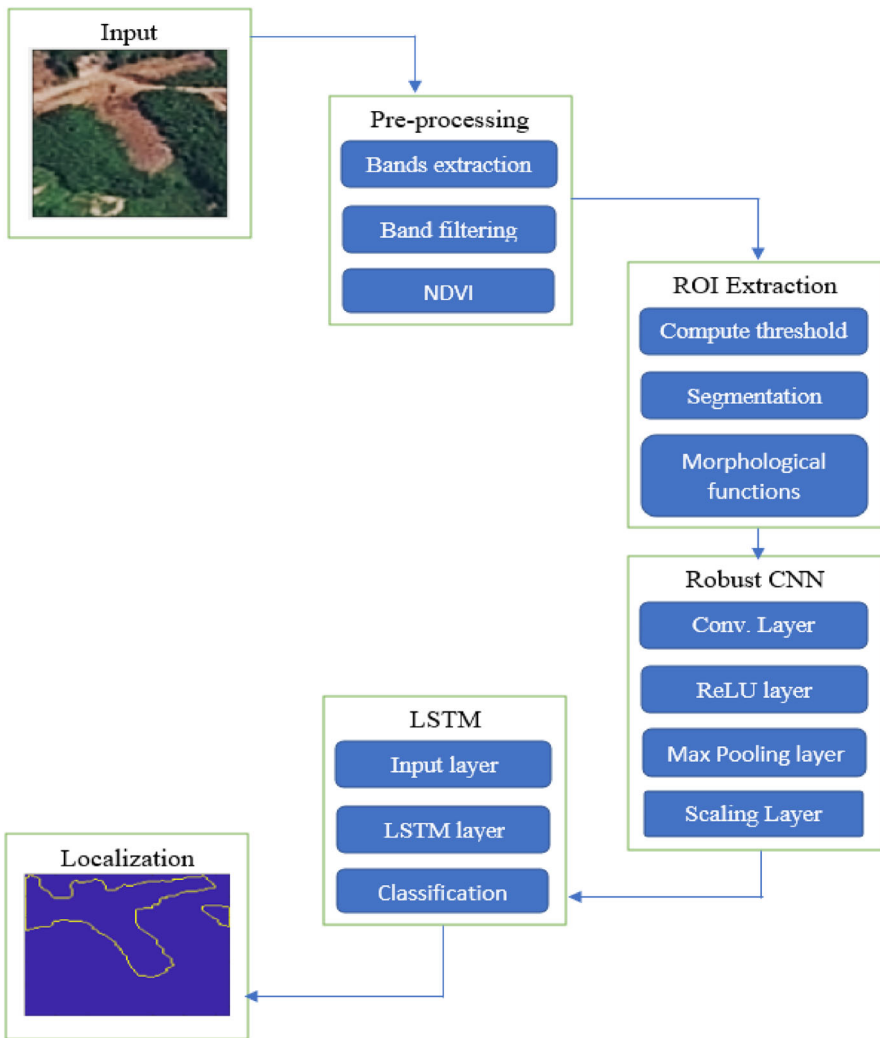


Fig. 1 Proposed architecture for automatic landslide prediction and localization

III satellite and are divided into two states: Maharashtra and Goa. The LISS-III images include four resolution bands: R, G, SWIR, and NIR [2]. Across the distinct periods, samples are collected for the landslide zones, which include pre-landslide and post-landslide. The whole specification of the obtained dataset is shown in Table 1.

Table 1 Dataset specification

| Regions        | Normal (pre-landslide) | Landslide (post-landslide) | Total samples |
|----------------|------------------------|----------------------------|---------------|
| Maharashtra    | 355                    | 1025                       | 1380          |
| Goa            | 355                    | 978                        | 1333          |
| Western Region | 710                    | 2003                       | 2713          |

### 3.2 Pre-processing

Computer vision algorithms are developed in this work to do pre-processing, ROI extraction, and feature extraction. Previously, we modified the LISS-3 sensor's input RS images geometrically and atmospherically. Geometric adjustments are made using the ERDAS tool's control points. The Chavez radiometric correction technique was used to the input RS image to reduce atmospheric influences. Then, using the adjusted RS image, we extract bands like visible NIR and visible R to do the NDVI. The pre-processing stage of NDVI is utilized to fine-tune the geometric regions, water, and vegetation. The steps below explain how the pre-processing phase works.

Let  $S$  is the input RS image collected from the LISS-3 satellite in the given study area. We corrected the initial geometric and atmospheric effects for each RS image  $S$  in the dataset. After that, we performed band extraction and NDVI computation. The NDVI of the  $S$  is computed using the spectral band R (3) and NIR (4).

$$R = \text{double}(S(:, :, 3)) \quad (1)$$

$$NIR = \text{double}(S(:, :, 4)) \quad (2)$$

We used 2D median filtering to denoise the image after extracting the 2D image bands. The median filtering method is used to eliminate noise from corrected bands. The 2D median filtering algorithm moves through the image pixel by pixel, replacing each value with the median value of the surrounding pixel. The size of the window determines the design of the neighbor. In this study, the window size of a 3-by-3 neighborhood is employed.

$$R1(i, j) = \text{median}\{R(i, j) | (i, j) \in w\} \quad (3)$$

$$NIR1(i, j) = \text{median}\{NIR(i, j) | (i, j) \in w\} \quad (4)$$

where,  $R1$  and  $NIR1$  is outcome of median filtering and  $w$  is the size of window. Finally, the we computed the NDVI by:

$$NDVI = \frac{(NIR1 - R1)}{(NIR1 + R1)} \quad (5)$$

Figures 2 and 3 demonstrate the visual results of the preceding stages for two RS images 1 and 2, respectively. The input RS image is represented as Coloured IR (CIR) in Figs. 2 and 3. This CIR image was already geometrically and atmospherically corrected. The visible red and NIR bands were extracted from the CIR image. The intrinsic noise components in these bands were suppressed via median filtering. Finally, the NDVI image had constructed by filtering the red and NIR bands.

### 3.3 Dynamic segmentation

The NDVI image is provided to the proposed dynamic segmentation method to extract the ROI. We used the simple dynamic threshold-based binary segmentation approach. The

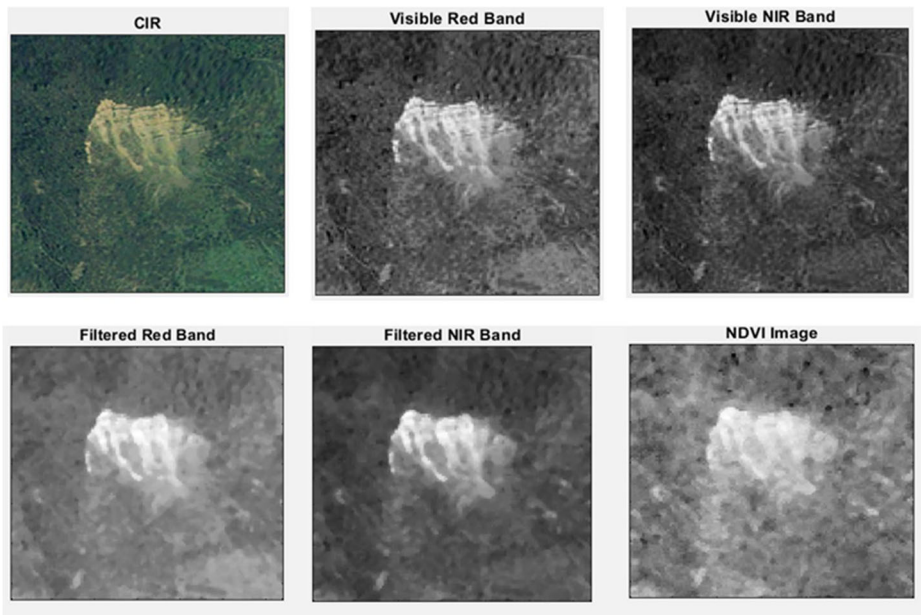


Fig. 2 Outcomes for the pre-processing of RS image 1

dynamic threshold for each input NDVI image is computed using the *graythresh* () MATLAB function. According to the threshold value, the rough ROI is extracted from the NDVI in binary form.

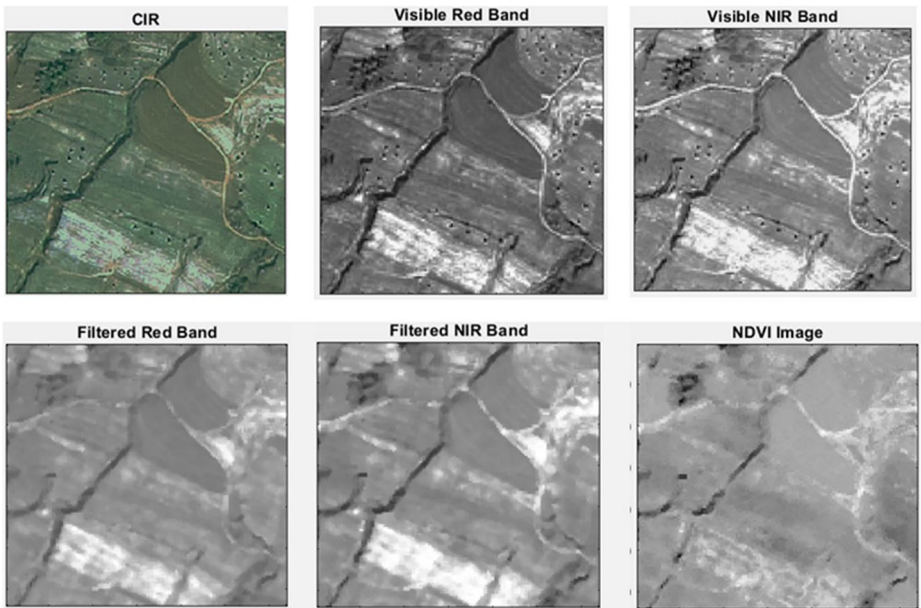


Fig. 3 Outcomes for the pre-processing RS image 2

$$t = \text{graythresh}(\text{NDVI}) \quad (6)$$

To estimate the ROI, the below steps are performed for NDVI of size  $m \times n$ .

$$\text{ROI} = (\text{NDVI}(i, j) > t), \quad i = 1, 2, \dots, m, j = 1, 2, \dots, n \quad (7)$$

where,  $t$  represents the threshold value,  $m$  represents the height of the image,  $n$  represents the width of the image,  $i$  represents the row pixel position, and  $j$  represents the column pixel position.

Unwanted items may be present in the ROI image. As a result, we used morphological techniques to improve the ROI output. The radius of the morphological disc structural element is set at 3. This structural component is critical in the morphological close process. The morphological closure operation is carried out using the result of the structural element (SE) function. The morphological close operation is a dilatation followed by an erosion, both of which use the same structural element. Equations (8) and (9) below summarise the steps.

$$\text{SE} = \text{strel}(\text{ROI}, 3) \quad (8)$$

where,  $\text{SE}$  represents the structuring element matrix and  $\text{strel}(\cdot)$  represents the morphological function to extract the  $\text{SE}$ .

Using this structuring of the element  $\text{SE}$ , we refine the current ROI image using the morphological close operation to produce the final ROI.

$$\text{ROI} = \text{imclose}(\text{ROI}, \text{SE}) \quad (9)$$

where, ROI represents the refined ROI image and  $\text{imclose}(\cdot)$  is morphological function to perform close operation.

### 3.4 Automatic features extraction

This section presents the proposed lightweight design of automatic feature extraction using the ResNet50 model. Figure 4 and Table 2 demonstrate the layers designed in the existing CNN model to reduce the computational efforts and increase the prediction accuracy. As shown in Fig. 4, the 2D ROI image is fed to the input layer of size  $224 \times 224$  of the CNN. After ROI extraction, we transformed the original size of the ROI image into  $224 \times 224$ . As this CNN model had designed using the ResNet 50 pre-trained system, it takes  $224 \times 224$  sized 2D images as input. The initial ResNet50 model is made up of 50 deep layers that were trained on the regular ImageNet dataset. ResNet50 is more powerful compared to other CNN models for automated feature extraction because of its quick processing speed and low memory needs.

To reduce the overall training and testing time, the CNN layers are designed in such a way that it takes minimum time. The proposed design consists of layers such as an input layer, convolutional layer (Conv), max-pooling layer (MPL), four residual blocks (Res), and Mean Normalized Pooling (MNP) layer. The Conv layer uses a variety of kernels to convolve the feature vectors to acquire high-level semiotic data. The max-pooling layer was then used to reduce the size of the Conv layer feature vectors. Every residual block (Res 1 to Res 4) has three blocks instead of two. Each residual block in the original ResNet-50 model comprises

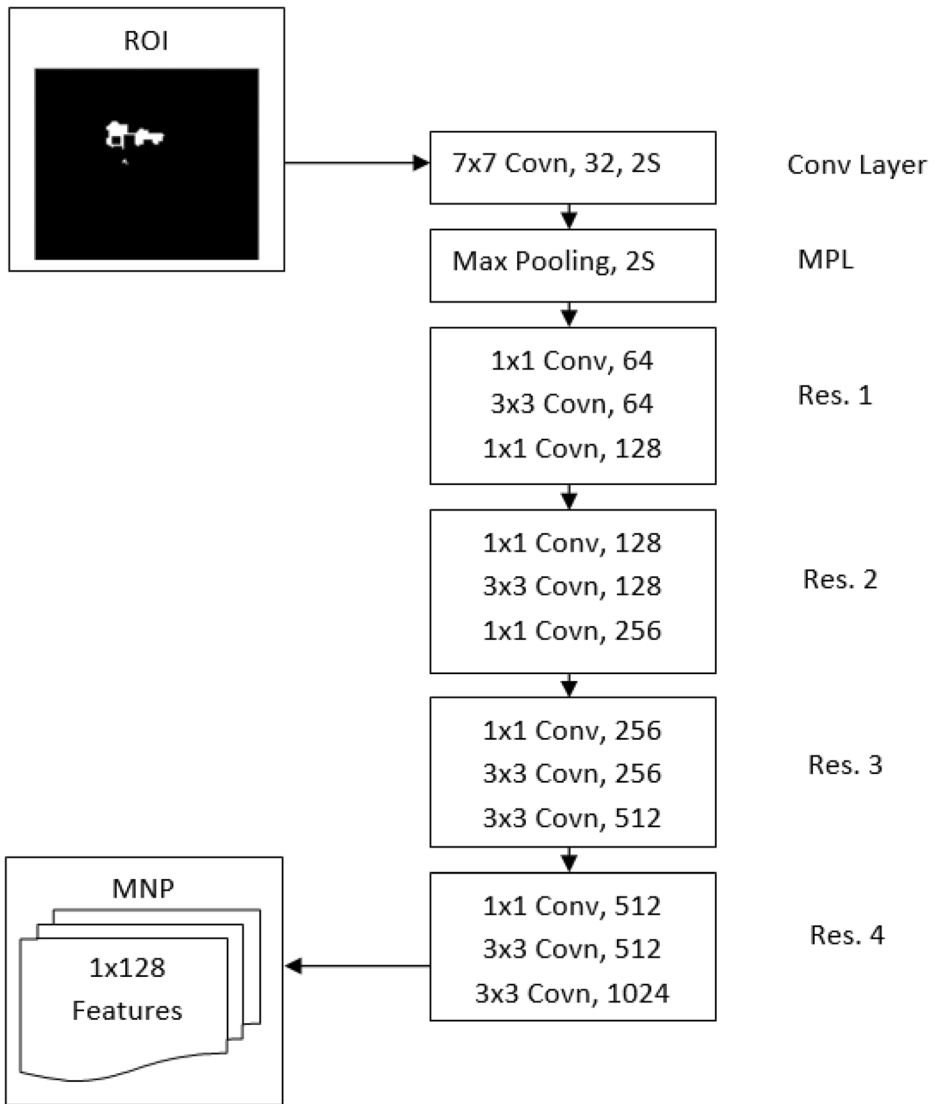


Fig. 4 Lightweight CNN layers design for features extraction

three stacked convolution layers, such as  $1 \times 1$ ,  $3 \times 3$ , and  $1 \times 1$ . The first  $1 \times 1$  Conv layer must lower the size of the feature vectors, the second  $3 \times 3$  Conv layer must estimate the feature vectors, and the third  $1 \times 1$  Conv layer must raise the dimension of the feature vectors again.

In a nutshell, the purpose of  $1 \times 1$  Conv filters is to minimize and increase the size of feature vectors. The number of filters in the original ResNet-50 model is more than in our proposed model. The original filters in ResNet-50 are 64 in the Conv layer, 128 filters in Res 1 block, 256 filters in Res 2 block, 512 filters in Res 3 block, and 1024 filters in Res 4 block. Whereas we modified the actual number of required filters in each layer by 50%, i.e., the number of filters in the Conv layer is set to 32. Therefore, it reduces the significant training

**Table 2** Configuration of proposed CNN layers

| Layer       | Layer Design   | Output Size |
|-------------|--|-------------|
| Input layer | Input layer (224, 224)   | 224×224     |
| Conv        | 32 7×7 Conv filters with Stride 2 (2S)   | 112×112     |
| MPL         | 3×3 max pool, 2S   | 112×112     |
| Res 1       | 64 1×1 Conv filters →ReLU 64 3×3 Conv filters →ReLU<br>128 1×1 Conv filters →ReLU    | 56×56       |
| Res 2       | 128 1×1 Conv filters →ReLU 128 3×3 Conv filters →ReLU<br>256 1×1 Conv filters →ReLU  | 28×28       |
| Res 3       | 256 1×1 Conv filters →ReLU 256 3×3 Conv filters →ReLU<br>512 1×1 Conv filters →ReLU  | 14×14       |
| Res 4       | 512 1×1 Conv filters →ReLU 512 3×3 Conv filters →ReLU<br>1024 1×1 Conv filters →ReLU | 7×7         |
| MNP         | Mean Normalize Pooling,  | 1×128       |

time and also reduces the number of extracted features for each input RS image. These adjusted residual blocks result in stable network operations with a well-balanced feature set. Each Conv layer is linked to the batch normalization layer for quick and efficient network training. Another unique element of the proposed CNN model is the use of a feature normalization method, known as MNP, in the final pooling layer. The  $1024 \times 1024$  high dimensional raw features matrix is delivered to this layer. We first transformed the  $2D 1024 \times 1024$  sized matrix into a  $1D 1024 \times 1$  matrix using mean operation. After that, we performed the feature selection using a Discrete Cosine Transform of size 128. It means DCT transforms the  $1024 \times 1$  matrix into a  $128 \times 1$  matrix. Finally, the  $128 \times 1$  feature vector has normalized using the min-max scaling approach.

The mathematical representation of the proposed CNN layers is represented below in Eq. (10). The input layer takes as input image ROI and performs the consolidated one squashing function as per the design of each layer:

$$F^{CNNl}_j = \tanh\left(\text{pool}_{\max}\left(\text{ReLU}\left(\sum_i y_j^{l-1}(ROI) * k_{ij}\right) + b_j^l\right)\right) \quad (10)$$

where,

- $F^{CNNl}_j$  is output of the Res.4 block using convolutional layer  $l$  of  $j^{\text{th}}$  input of size 2D.
- $y_j^{l-1}$  represents the previous convolutional layer features maps of ROI,
- $k_{ij}$  represents  $i^{\text{th}}$  trained convolutional kernels,
- $b_j^l$  represents the additive bias.
- $\tanh(\cdot)$  represents the activation function,
- $\text{pool}_{\max}(\cdot)$  represents the operation of max pooling for features extraction,
- $\text{ReLU}(\cdot)$  represents the operation of ReLU layer.

After that, we applied the final layer MNP to estimate the robust, reduced, and normalized CNN feature for the input ROI image using next steps. We first applied the mean function in Eq. (11).

$$F^{\text{mean}} = \text{mean}(F^{CNN}) \quad (11)$$

Then, the feature selection using DCT performed in Eq. (12):

$$F^{dct} = dct(F^{mean}, 128) \tag{12}$$

Due to considerable variability, a feature requires a longer convergence time for neural networks. As a result, features scaling is necessary to improve speed and accuracy. In this research, we used the min-max normalisation strategy as showing in Eq. (13), which scales each feature from 0 to 1.

$$F = \frac{(F^{dct} - \min(F^{dct}))}{(\max(F^{dct}) - \min(F^{dct}))} \tag{13}$$

### 3.5 Landslide prediction

The next step of the proposed model is belonging to the prediction of the landslide that takes inputs F of test RS image and pre-trained proposed CNN model. For the prediction, we designed the deep learning classifier LSTM. As the dataset is divided into 70% training and 30% testing, the classier LSTM performs the classification of the 30% RS samples. As the conventional classifiers such as ANN and SVM suffered from higher training and classification errors due to vanishing gradient points, the LSTM deep learning classifier is preferred in this paper. We introduced the LSTM classifier connected with the proposed CNN model. The CNN does the automatic feature extraction and fed to the LSTM for the prediction for each input RS image. Compare to SVM and ANN, LSTM also has minimum computational complexity.

LSTM also consists of different layers for sequential learning and classification. LSTM input layer receives F at current time interval  $t$ . LSTM layer is made up of input gate  $i$ , output gate  $o$ , and forget gate  $f$ , and a memory cell  $c$ . For every time  $t$ , LSTM computes activations of its gates  $\{i_t, f_t\}$  and updates its memory cell from  $c_{t-1}$  to  $c_t$ , it then computes the activation of output gate  $o_t$ , and finally outputs a hidden representation  $h_t$ . The hidden representation from the previous time step is  $h_{t-1}$ . Following equations applied in LSTM for update functions:

$$i_t = \sigma(W_i Fr + U_i h_{t-1} + V_i c_{t-1} + b_i) \tag{14}$$

$$f_t = \sigma(W_f Fr + U_f h_{t-1} + V_f c_{t-1} + b_f) \tag{15}$$

$$c_t = f_t \Theta c_{t-1} + i_t \Theta \tanh(W_c Fr + U_c h_{t-1} + U_c h_{t-1}) \tag{16}$$

$$o_t = \sigma(W_o Fr + U_o h_{t-1} + V_o c_{t-1} + b_o) \tag{17}$$

$$h_t = o_t \Theta \tanh(c_t) \tag{18}$$

where,  $\Theta$  represents an element-wise product,  $\sigma$  represents the logistic function, and  $\tanh$  represents the activation function.  $W_*$ ,  $V_*$ ,  $U_*$ , and  $b_*$  represents the parameters at different gates, and  $V_*$  represents the weight matrix. The classification layer estimates the probabilities

for each class and predicts the final prediction outcome. While for LSTM training, we set the number of hidden layers to 50, the number of epochs to 50, minimum batch size 20, and gradient threshold 10. The average training period using the proposed model was 3678 seconds, and the number of training iterations required was 68. For the comparative study, we have trained SVM and ANN classifiers on the CNN features using 10-cross fold validation and 10 hidden layered backpropagation neural network, respectively.

### 3.6 Landslide region localization

Landslide localization is yet another vital research challenge. With the prediction of landslide possibility, it will be interesting if the exact landslide regions will be localized for the appropriate conditions monitoring in real-time. In this paper, if the outcome of the prediction step is landslide prediction, then we initiate the landslide region localization. According to the result of landslide prediction, we utilized the ROI outcome and original CIR image as input to localize the predicted landslide region. However, the ROI extracted from the NDVI image is not sufficient for the accurate localization of landslide regions. Therefore, we further computed the Normalized Difference Water Index (NDWI) using the median filtered green band and NIR band. Figure 5 shows the functionality of the landslide localization. It is a relatively easy method for locating landslide areas if the landslide is anticipated by the classifiers. It takes inputs of median filtered R, G, and NIR bands. For NDVI, we already had outputs like the NDVI image and its ROI extraction using the dynamic segmentation technique using Eq. (5) and Eq. (9) respectively. During localization, we directly refer to the output of Eq. (9) as the

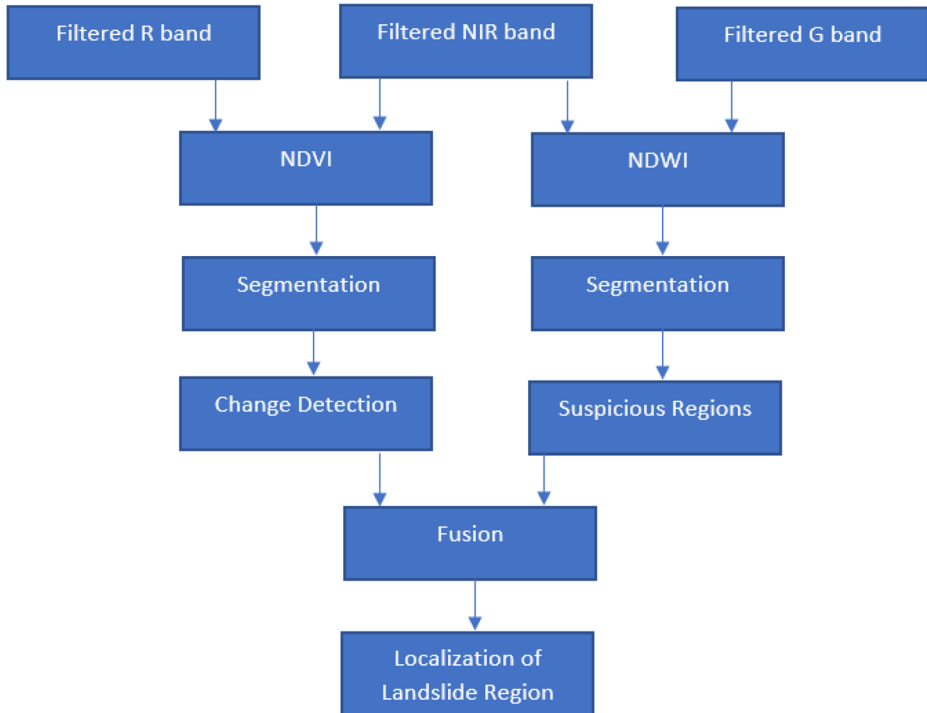


Fig. 5 Proposed architecture for the landslide region localization

change detection output in the localization phase. For suspicious regions discovery, we have computed the NDWI using the filtered G and NIR bands using Eq. (19).

$$NDWI = \frac{(G1 - NIR1)}{(G1 + NIR1)} \quad (19)$$

where, G1 is the median filtered 2D image of original G Band.

The dynamic threshold-based segmentation using Eq. (6)–(9) is applied on the NDWI image to find the suspicious zone. Finally, the final localization output image was created by fusing the change detection output and suspicious region detection images. Figure 6 depicts the results of the proposed landslide regions localization. It displays the results of NDVI segmentation (also known as change detection) and NDWI segmentation (we named it suspicious regions detection). Then, both outputs were fused to display them as changes in detected areas. Finally, the landslide region is located using morphological techniques such as identifying the perimeter of an item in a binary image.

## 4 Simulation results

A well-known image processing program, MATLAB, was used to build the suggested model, as previously indicated. The Windows 10 operating system, 8 GB of RAM, and an Intel I5 CPU were used in the implementation. Analysis of performance for Western India was carried out utilizing the dataset previously discussed in this paper. Each RS image has 2713 landslide zones in Maharashtra and Goa that were image graphed. The dataset had been divided into two categories: training samples (70%) and testing samples (30%). The accuracy, f1-score, precision, recall, and specificity of the five-performance metrics were evaluated after 30% of the samples were classified using different classifiers LSTM, ANN, and SVM. We achieved this by analyzing the parameters of the confusion matrix. Formulas to calculate these parameters are accessible in a significant number of research. We first investigate the performances of SVM, ANN, and LSTM classifiers on the proposed model. Then study the comparative study of the proposed model with state-of-the-art techniques.

### 4.1 Performance investigations

In this paper, we proposed a fully automated model using CNN and LSTM approaches. To claim the efficiency of the proposed model, we conducted two-fold comparative investigations. First, we analyzed the comparative analysis among the LSTM, SVM, and ANN classifiers. Secondly, we analyzed the raw CNN features (without the MNP layer) and

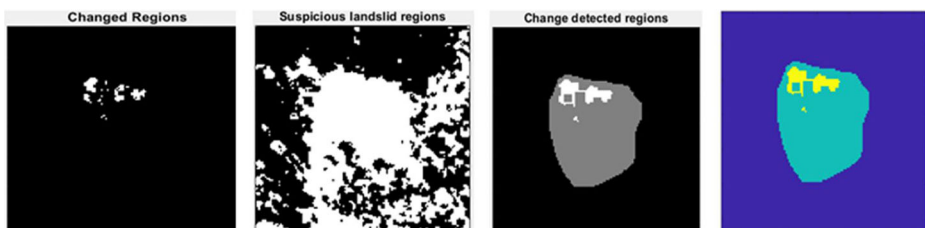


Fig. 6 Example of landslide regions localization for input RS image 1

normalized CNN features (proposed CNN model shown in Fig. 4 and Table 2). We have fed these two types of CNN features to three classifiers ANN, SVM, and LSTM. According to each classifier outcome, we have measured the performances of landslide prediction using five performance metrics. Figures 7, 8, 9, 10 and 11 show the performances for prediction accuracy, prediction F1-score, precision, recall, and specificity rates using each classifier with raw CNN and normalized CNN features. Here, the raw CNN features themselves represent the existing CNN model also. Therefore, this study indirectly investigates the performance of the proposed CNN model (Normalized CNN features) with the underlying CNN model (raw CNN features).

Figures 7 and 8 illustrate prediction accuracy and F1-score results utilizing the ANN SVM and LSTM with raw CNN and normalized CNN features, respectively. Regardless of the kind of CNN features provided to LSTM, it outperformed the ANN and SVM classifiers. It is due to the superiority of the deep learning classifier LSTM over the conventional ANN and SVM classifiers. LSTMs are a form of RNN that can handle exploding and vanishing gradient issues. It is usually supplemented with repeated gates known as forget gates. Unlike SVM and prior neural networks like ANN, LSTM can perform deep learning tasks that demand a long-term recall of events. Therefore, LSTM shows a significant performance improvement over the SVM and ANN. Among SVM and ANN, noticed that the ANN classifier shows improved accuracy performance over the SVM classifier. The cause for the higher ANN accuracy is that effectively addressed the non-linear problems over the SVM classifier. The kernel function is the key in SVM since it uses nonlinear mapping to make the data linearly separable. To cope with nonlinear issues, however, ANN uses multi-layer connections and multiple activation functions. It increases the ANN's overall prediction performance compared to the SVM classifier, independent of the type of features used for training and testing.

Similar to accuracy and F1-score performances, the precision rate in Fig. 9, the recall rate in Fig. 10, and the specificity rate in Fig. 11 demonstrate that LSTM outperformed the ANN and SVM classifiers for both raw and normalized CNN features. The maximum accuracy for the ANN classifier was 90.67%, the SVM classifier was 88.42%, and the LSTM classifier was

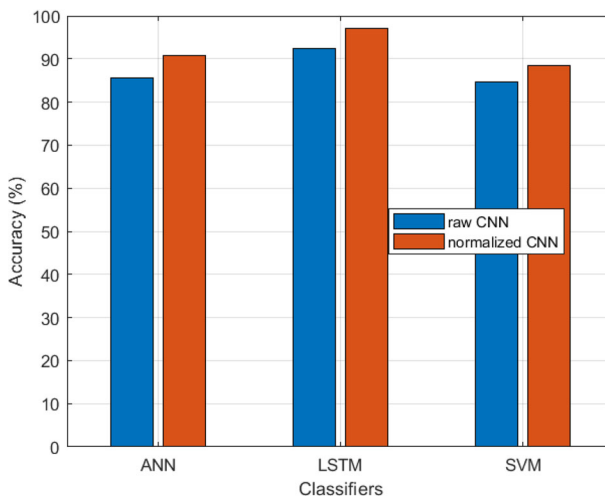
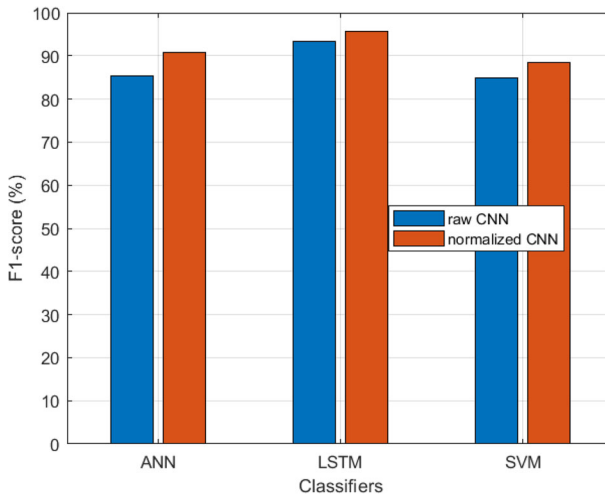


Fig. 7 Prediction accuracy analysis using different classifiers



**Fig. 8** Prediction F1-score using different classifiers

97.03. Similarly, the maximum F1 score for the ANN classifier was 90.72%, the SVM classifier was 88.51%, and the LSTM classifier was 95.73.

Apart from the investigation of the classifier's performances, the outcomes in Figs. 7, 8, 9, 10 and 11 also demonstrate the analysis of the raw CNN and normalized CNN features. We investigated the existing CNN model and proposed the CNN model to access the impact of using them on the overall prediction performances. From the achieved outcomes, it is observed that normalized CNN features produced improved prediction results compared to the raw CNN features. There are various reasons for such performance improvement such as (1) high-dimension raw CNN features contain several irrelevant and redundant features that increase the classification errors, (2) the proposed CNN model performed the raw CNN features reduction using mean and DCT functions, (3) the raw CNN features contains severe variations in the value of their features that poorly affects the prediction outcomes, and (4) the scaled

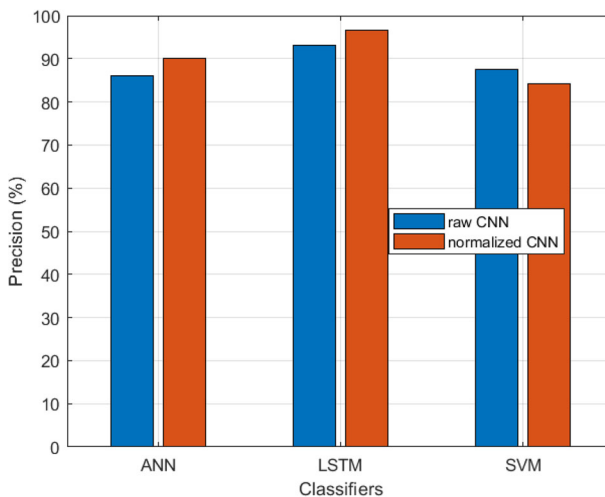


**Fig. 9** Precision analysis using different classifiers

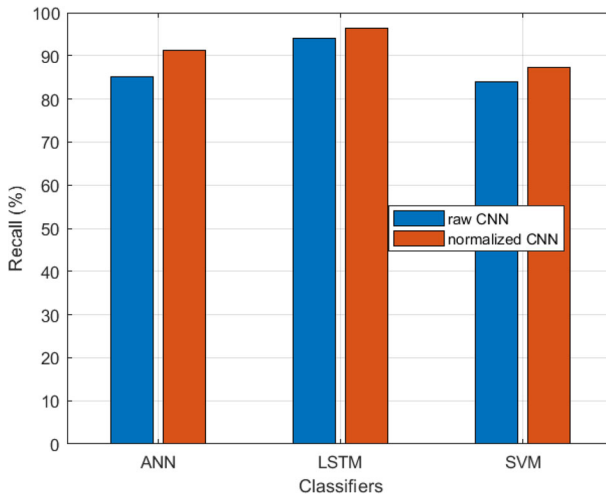


**Fig. 10** Recall analysis using different classifiers

features using the min-max normalization brings all features in the particular range which boosts the performances of the classifiers. Tables 3 and 4 presents the outcomes that demonstrate the classifiers evaluation and CNN features evaluation to confirm the efficiency of the proposed CNN-LSTM model for landslide prediction. Table 3 claims that the proposed CNN-LSTM model has improved the overall performance approximately by 6% compared to SVM and ANN models. Table 4 claims that the normalized CNN features with LSTM have improved the overall performance approximately by 5% compared to raw CNN features.

## 4.2 State-of-the-art analysis

This section presents the comparative study of the proposed model with a recent deep learning-based approach for landslide prediction. We have implemented existing deep learning-based

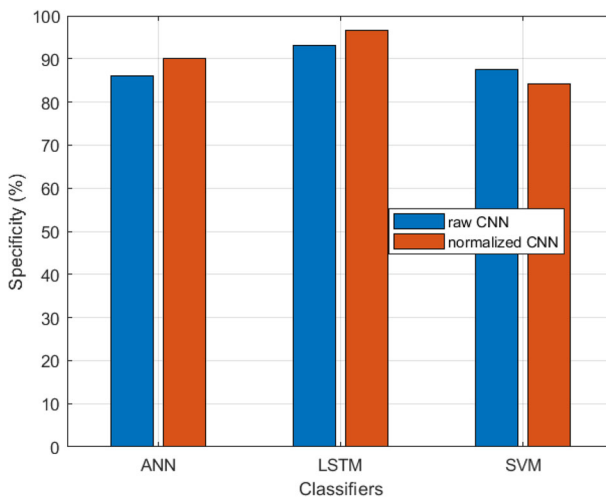


**Fig. 11** Specificity analysis using different classifiers

**Table 3** Comparative analysis of classifiers using normalized CNN features

| Measures        | SVM   | ANN   | LSTM  |
|-----------------|-------|-------|-------|
| Accuracy (%)    | 88.42 | 90.67 | 97.03 |
| F1-score (%)    | 88.51 | 90.72 | 95.73 |
| Precision (%)   | 84.25 | 90.17 | 96.16 |
| Recall (%)      | 89.67 | 91.17 | 96.28 |
| Specificity (%) | 84.25 | 90.17 | 96.6  |

methods using a similar dataset under the same system configurations to investigate the three core performance metrics such as prediction accuracy, prediction F1-score, average training time, and average prediction time. We have compared the performance of the proposed model with four state-of-the-art techniques as Bui et al. [5], Azarafza et al. [2], Qin et al. [27], and Thi et al. [38]. The results in Table 5 show the proposed model reduced the overall training and prediction time significantly compared to other similar methods. It shows that the proposed model can minimize computational efforts by 35% compared to existing deep learning techniques. On the other side, the prediction accuracy and F1-score performances also showed improvement using the proposed model compared to all state-of-the-art methods.

The proposed model for landslide prediction and localization has improved the performance of existing solutions due to steps such as pre-processing, ROI extraction, lightweight feature extraction, and LSTM classification. The pre-processing approach removed the atmospheric and geometric effects to overcome the misclassification problems. The landslide regions extraction from the pre-processed RS image helps to estimate the unique and region-specific features automatically. The lightweight CNN layers lead to a reduction in overall processing time with optimal prediction accuracy. As the high-dimension raw CNN features contain several irrelevant and redundant features that increase the classification errors, we have performed the features selection and normalization to improve the accuracy. The normalized features using the min-max normalization bring all features in the particular range which boosts the performances of the classifiers.

## 5 Conclusion and future work

According to current research problems described in this paper, a novel framework for automatic landslide prediction with landslide region localization had proposed. The real-time RS-based landslide prediction and localization suffered from various challenges. The lack of prominent real-time RS images dataset problem had addressed by collecting the RS images for Maharashtra and Goa landslide regions in this research work. The problem with underlying

**Table 4** Comparative analysis of raw and normalized features using LSTM

| Measures        | Raw CNN | Normalized CNN |
|-----------------|---------|----------------|
| Accuracy (%)    | 92.39   | 97.03          |
| F1-score (%)    | 93.43   | 95.73          |
| Precision (%)   | 92.89   | 96.16          |
| Recall (%)      | 93.98   | 96.28          |
| Specificity (%) | 93.01   | 96.6           |

**Table 5** State-of-the-art comparative analysis

| Methods             | Accuracy (%) | F1-score (%) | Average Training Time (Seconds) | Average Prediction Time (Sec.) |
|---------------------|--------------|--------------|---------------------------------|--------------------------------|
| Bui et al. [5]      | 94.34        | 93.67        | 5788                            | 15.93                          |
| Azarafza et al. [2] | 95.39        | 94.34        | 5473                            | 13.44                          |
| Qin et al. [27]     | 95.88        | 95.12        | 5983                            | 17.49                          |
| Thi et al. [38]     | 93.40        | 93.23        | 5348                            | 12.39                          |
| Proposed            | 97.03        | 95.73        | 3678                            | 9.34                           |

methods was the lack of an appropriate mechanism to remove the atmospheric modifications, geometric corrections, or superfluous areas from the raw RS images. We pre-processed each RS image to remove atmospheric and geometric corrections using band filtering and the NDVI approach. The ROI was extracted from the NDVI image using a dynamic segmentation approach. The high complexity deep learning models for landslide prediction was another problem that we addressed by presenting a novel CNN framework for automatic feature extraction. The proposed CNN model with features reduction and normalization leads to lower computational requirements and higher prediction accuracy. Finally, the classifications were performed using the LSTM, SVM, and ANN classifiers. The experimental results prove the efficiency of the proposed model improves the overall accuracy by 2% while reducing the computational time by 35% compared to state-of-the-art techniques. In this paper, we have designed the post-processing step also to localize the predicted landslide regions. For future work, we recommend the work on landslide region localization with more investigation in terms of performance metrics and similar methods of analysis.

**Data availability** Data sharing not applicable to this article as no datasets were generated or analyzed during the current study.

## Declarations

**Ethical approval** This article does not contain any studies with human participants performed by any of the authors.

**Conflict of interest** All authors declares that they has no conflict of interest.

## References

1. Aksoy B, Ercanoglu M (2012) Landslide identification and classification by object-based image analysis and fuzzy logic: an example from the Azdavay region (Kastamonu, Turkey). *Comput Geosci* 38(1):87–98. <https://doi.org/10.1016/j.cageo.2011.05.010>
2. Azarafza M, Azarafza M, Akgün H, Atkinson PM, Derakhshani R (2021) Deep learning-based landslide susceptibility mapping. *Sci Rep* 11:24112. <https://doi.org/10.1038/s41598-021-03585-1>
3. Bakkouri I, Afdel K (2020) Computer-aided diagnosis (CAD) system based on multi-layer feature fusion network for skin lesion recognition in dermoscopy images. *Multimed Tools Appl* 79:20483–20518. <https://doi.org/10.1007/s11042-019-07988-1>
4. Bakkouri I, Afdel K, Benois-Pineau J, Initiative GCFA (2022) BG-3DM2F: bidirectional gated 3D multi-scale feature fusion for Alzheimer’s disease diagnosis. *Multimed Tools Appl* 81:10743–10776. <https://doi.org/10.1007/s11042-022-12242-2>
5. Bui T-A, Lee P-J, Lum K-Y, Loh C, Tan K (2020) Deep learning for landslide recognition in satellite architecture. *IEEE Access* 8:143665–143678. <https://doi.org/10.1109/access.2020.3014305>

6. Chang H-H, Chan W-C (2021) Automatic Registration of Remote Sensing Images Based on Revised SIFT With Trilateral Computation and Homogeneity Enforcement. *IEEE Trans Geosci Remote Sens*:1–16. <https://doi.org/10.1109/TGRS.2021.3052926>
7. Das I, Stein A, Kerle N et al (2011) Probabilistic landslide hazard assessment using homogeneous susceptible units (HSU) along a national highway corridor in the northern Himalayas. *India Landslides* 8: 293–308. <https://doi.org/10.1007/s10346-011-0257-9>
8. Deep learning algorithms for medical image processing. *Multimed Tools Appl* 79, 9845 (2020). <https://doi.org/10.1007/s11042-020-08673-4>.
9. Ghorbanzadeh O, Shahabi H, Crivellari A, Homayouni S, Blaschke T, Ghamisi P (2022) Landslide detection using deep learning and object-based image analysis. *Landslides* 19:929–939. <https://doi.org/10.1007/s10346-021-01843-x>
10. Hwang S, Guevarra IF, Yu B (2009) Slope failure prediction using a decision tree: a case of engineered slopes in South Korea. *Eng Geol* 104(1–2):126–134. <https://doi.org/10.1016/j.enggeo.2008.09.004>
11. Khalifa NE, Loey M, Mirjalili S (2022) A comprehensive survey of recent trends in deep learning for digital images augmentation. *Artif Intell Rev* 55:2351–2377. <https://doi.org/10.1007/s10462-021-10066-4>
12. Khanlari GR, Heidari M, Momeni AA, Abdilor Y (2012) Prediction of shear strength parameters of soils using artificial neural networks and multivariate regression methods. *Eng Geol* 131–132:11–18. <https://doi.org/10.1016/j.enggeo.2011.12.006>
13. Lee S, Min K (2001) Statistical analysis of landslide susceptibility at Yongin, Korea. *Environ Geol* 40(9): 1095–1113. <https://doi.org/10.1007/s002540100310>
14. Lee S, Hwang J, Park I (2013) Application of data-driven evidential belief functions to landslide susceptibility mapping in Jinju, Korea. *CATENA* 100:15–30. <https://doi.org/10.1016/j.catena.2012.07.014>
15. Li L, Cheng S, Wen Z (2021) Landslide prediction based on improved principal component analysis and mixed kernel function least squares support vector regression model. *J Mt Sci* 18:2130–2142. <https://doi.org/10.1007/s11629-020-6396-5>
16. Lu W, Zhao L, Xu R (2021) Remote sensing image processing technology based on mobile augmented reality technology in surveying and mapping engineering. *Soft Comput* 27:423–433. <https://doi.org/10.1007/s00500-021-05650-3>
17. Marjanović M, Kovačević M, Bajat B, Voženilek V (2011) Landslide susceptibility assessment using SVM machine learning algorithm. *Eng Geol* 123(3):225–234. <https://doi.org/10.1016/j.enggeo.2011.09.006>
18. Meena SR, Soares LP, Grohmann CH, van Westen C, Bhuyan K, Singh RP, Floris M, Catani F (2022) Landslide detection in the Himalayas using machine learning algorithms and U-net. *Landslides* 19:1209–1229. <https://doi.org/10.1007/s10346-022-01861-3>
19. Mohan A, Kumar B, Dwivedi R (2021) Review on remote sensing methods for landslide detection using machine and deep learning. *Trans Emerg Telecommun Technol* 32. <https://doi.org/10.1002/ett.3998>
20. Nanare I, Bhooyar D, Balamwar S (2021) Remote sensing satellite image analysis for deforestation in Yavatmal District, Maharashtra, India. 684–688. <https://doi.org/10.1109/ICSPC51351.2021.9451744>
21. Nhu V-H, Shirzadi A, Shahabi H, Singh SK, Al-Ansari N, Clague JJ, Jaafari A, Chen W, Miraki S, Dou J, Luu C, Górski K, Thai Pham B, Nguyen HD, Ahmad BB (2020) Shallow landslide susceptibility mapping: a comparison between logistic model tree, logistic regression, Naïve Bayes tree, artificial neural network, and support vector machine algorithms. *Int J Environ Res Public Health* 17(8):2749. <https://doi.org/10.3390/ijerph17082749>
22. Pain CD, Egan GF, Chen Z (2022) Deep learning-based image reconstruction and post-processing methods in positron emission tomography for low-dose imaging and resolution enhancement. *Eur J Nucl Med Mol Imaging* 49:3098–3118. <https://doi.org/10.1007/s00259-022-05746-4>
23. Parsa M, Maghsoudi A, Shokouh B (2014) Landslide Susceptibility Mapping of Komroud Sub-basin Using Fuzzy Logic Approach 02
24. Pawluszek K, Marczak S, Borkowski A, Tarolli P (2019) Multi-aspect analysis of object-oriented landslide detection based on an extended set of LiDAR-derived terrain features. *ISPRS Int J Geo Inf* 8(8):321. <https://doi.org/10.3390/ijgi8080321>
25. Perkins S (2012) Death toll from landslides vastly underestimated. <http://www.nature.com/>. <http://www.emdat.be/database>.
26. Pradhan B (2013) A comparative study on the predictive ability of the decision tree, support vector machine and neuro-fuzzy models in landslide susceptibility mapping using GIS. *Comput Geosci* 51:350–365. <https://doi.org/10.1016/j.cageo.2012.08.023>
27. Qin S, Guo X, Sun J, Qiao S, Zhang L, Yao J, Cheng Q, Zhang Y (2021) Landslide detection from open satellite imagery using distant domain transfer learning. *Remote Sens* 13:3383. <https://doi.org/10.3390/rs13173383>
28. Rasyid AR, Bhandary NP, Yatabe R (2016) Performance of frequency ratio and logistic regression model in creating GIS based landslides susceptibility map at Lompobattang Mountain, Indonesia. *Geoenviron Disasters* 3:19. <https://doi.org/10.1186/s40677-016-0053-x>

29. Roy J, Saha S (2019) Landslide susceptibility mapping using knowledge driven statistical models in Darjeeling District, West Bengal, India. *Geoenviron Disasters* 6:11. <https://doi.org/10.1186/s40677-019-0126-8>
30. Sajadi P, Sang Y-F, Gholamnia M, Bonafoni S (2022) Evaluation of the landslide susceptibility and its spatial difference in the whole Qinghai-Tibetan plateau region by five learning algorithms. *Geoscience Letters* 9. <https://doi.org/10.1186/s40562-022-00218-x>
31. San BT (2014) An evaluation of SVM using polygon-based random sampling in landslide susceptibility mapping: the Candir catchment area (western Antalya, Turkey). *Int J Appl Earth Obs Geoinf* 26:399–412. <https://doi.org/10.1016/j.jag.2013.09.010>
32. Sarker IH (2021) Deep learning: a comprehensive overview on techniques, taxonomy, applications and research directions. *SN Comput sci* 2:420. <https://doi.org/10.1007/s42979-021-00815-1>
33. Sezer E, Pradhan B, Gokceoglu C (2011) Manifestation of an adaptive neuro-fuzzy model on landslide susceptibility mapping: Klang valley, Malaysia. *Expert Syst Appl* 38:8208–8219. <https://doi.org/10.1016/j.eswa.2010.12.167>
34. Shahabi H, Hashim M (2015) Landslide susceptibility mapping using GIS-based statistical models and remote sensing data in tropical environment. *Sci Rep* 5:9899. <https://doi.org/10.1038/srep09899>
35. Shahabi H, Rahimzad M, Tavakkoli Piraililou S, Ghorbanzadeh O, Homayouni S, Blaschke T, Lim S, Ghamisi P (2021) Unsupervised deep learning for landslide detection from multispectral Sentinel-2 imagery. *Remote Sens* 13(22):4698. <https://doi.org/10.3390/rs13224698>
36. Srivastava P, Shukla A, Bansal A (2021) A comprehensive review on soil classification using deep learning and computer vision techniques. *Multimed Tools Appl* 80:14887–14914. <https://doi.org/10.1007/s11042-021-10544-5>
37. Tavakkoli Piraililou S, Shahabi H, Jarhani B, Ghorbanzadeh O, Blaschke T, Gholamnia K, Meena S, Aryal J (2019) Landslide detection using multi-scale image segmentation and different machine learning models in the higher Himalayas. *Remote Sens* 11(21):2575. <https://doi.org/10.3390/rs11212575>
38. Thi Ngo PT, Panahi M, Khosravi K, Ghorbanzadeh O, Karimnejad N, Cerda A, Lee S (2020) Evaluation of deep learning algorithms for national scale landslide susceptibility mapping of Iran. *Geosci Front* 12:505–519. <https://doi.org/10.1016/j.gsf.2020.06.013>
39. Tien Bui D (2012) Modeling of rainfall-induced landslide hazard for the Hoa Binh, province of Vietnam. Norwegian University of Life Sciences. Ph. D Thesis
40. Ulló SL, Langenkamp MS, Oikarinen TP, DelRosso MP, Sebastianelli A, Piccirillo FP, Sica S (2019) Landslide Geohazard Assessment with Convolutional Neural Networks Using Sentinel-2 Imagery Data. *IGARSS 2019–2019 IEEE International Geoscience and Remote Sensing Symposium*. <https://doi.org/10.1109/igarss.2019.8898632>
41. Wang Y, Wang X, Jian J (2019) Remote sensing landslide recognition based on convolutional neural network. *Math Probl Eng* 2019:1–12. <https://doi.org/10.1155/2019/8389368>
42. Wang H, Zhang L, Yin K, Luo H, Li J (2020) Landslide identification using machine learning. *Geosci Front* 12:351–364. <https://doi.org/10.1016/j.gsf.2020.02.012>
43. Wang Y, Wen H, Sun D, Li Y (2021) Quantitative assessment of landslide risk based on susceptibility mapping using random Forest and GeoDetector. *Remote Sens* 13(13):2625. <https://doi.org/10.3390/rs13132625>
44. Yalcin A, Reis S, Aydinoglu A, Yomralioglu T (2011) A GIS-based comparative study of frequency ratio, analytical hierarchy process, bivariate statistics and logistics regression methods for landslide susceptibility mapping in Trabzon, NE Turkey. *CATENA* 85:274–287. <https://doi.org/10.1016/j.catena.2011.01.014>
45. Yang G, Liu J, Qu M, Wang S, Ye D, Zhong H (2021) FaasRS: Remote Sensing Image Processing System on Serverless Platform. 258–267. <https://doi.org/10.1109/COMPSAC51774.2021.00044>
46. Ye C, Wei R, Ge Y et al (2022) GIS-based spatial prediction of landslide using road factors and random forest for Sichuan-Tibet Highway. *J Mt Sci* 19:461–476. <https://doi.org/10.1007/s11629-021-6848-6>

**Publisher's note** Springer Nature remains neutral with regard to jurisdictional claims in published maps and institutional affiliations.

Springer Nature or its licensor (e.g. a society or other partner) holds exclusive rights to this article under a publishing agreement with the author(s) or other rightsholder(s); author self-archiving of the accepted manuscript version of this article is solely governed by the terms of such publishing agreement and applicable law.